Turkish Journal of Chemistry

http://journals.tubitak.gov.tr/chem/

Research Article

Turk J Chem
(2020) 44: 448 – 460
© TÜBİTAK
doi:10.3906/kim-1910-21

Preparation and catalytic evaluation of Au/γ-Al_2O_3 nanoparticles for the conversion of 4-nitrophenol to 4-aminophenol by spectrophotometric method

Farhat SAIRA[1], **Naveeda FIRDOUS**[2], **Rumana QURESHI**[2,*], **Ayesha IHSAN**[3]

[1]Nanoscience and Technical Division, National Centre for Physics (NCP), Shahdra Valley Rd, Islamabad, Pakistan

[2]Department of Chemistry, Quad-i-Azam University, Islamabad, Pakistan

[3]National Institute of Biotechnology and Genetic Engineering (NIBGE), Faisalabad, Pakistan

Received: 08.10.2019 • **Accepted/Published Online:** 14.02.2020 • **Final Version:** 01.04.2020

Abstract: A set of catalysts having gold nanoparticles deposited on γ-Al_2O_3 (Au/ γ-Al_2O_3) with lowest effective amount of gold content were prepared by successive impregnation and hydrogen reduction method. The structural features of prepared catalysts were analysed by X-ray diffraction (XRD), N_2 physisorption, scanning electron microscopy (SEM), and Fourier transform infrared (FTIR). The catalytic activity was evaluated for the reduction of an organic pollutant 4-nitrophenol (4NP) to 4-aminophenol (4AP) by spectrophotometric analysis. Supported catalyst presented excellent catalytic ability to convert 4NP to 4AP in the presence of sodium borohydride (SBH) due to synergistic effect of Au NPs and mesoporous γ-Al_2O_3 support. The reduction reaction was also performed at a range of temperatures to calculate kinetic parameters. The development of highly stable Au/γ-Al_2O_3 catalysts with lowest noble metal content and recyclability made the process cost effective and may promote their applications in various fields including removal of organic pollutants in industrial waste water and high-temperature gas-phase reactions.

Key words: Gold catalyst, γ-Al_2O_3, UV-visible spectroscopy, 4-Nitrophenol

1. Introduction

Supported gold catalysts are currently being used to catalyse various reactions having environmental and industrial significance. The incredible catalytic activity of supported gold nanoparticles (NPs) was first identified by Haruta et al. [1]. Since then, gold NPs have been used as a catalyst in many reactions involving electron transfer process [2-6].

Industrially important catalytic processes mainly require stable supported metal or metal oxide catalysts [7]. The advantages of supported metal catalysts are the uniform metal distribution, no agglomeration, and deposition of less metal content on the support, easy recovery of expensive noble metal, multiple uses of the catalysts, and cost economics [8]. The catalytic performance of a metal deposited on a support depends on the properties of support as well as active metal [9,10]. The support can play a crucial role in understanding the catalytic phenomenon including diffusion of reactants [11,12], metal-support interactions [13,14], hydrophilic character of catalyst [15] etc. Gold NPs have been supported on multiple supports including silica, titania, mixed oxides, zeolites, boehmite, and alumina [16–20]. The most commonly used catalytic support is γ-Al_2O_3 due to its high surface area and porosity, optimum mechanical strength, and uniform pore size distribution [21].

*Correspondence: r_quresh@qau.edu.pk

Typically, impregnation method is employed for the preparation of supported catalysts. It is based on soaking the support into metal salt solution followed by evaporation and metal reduction. A surfeit of reports on the catalytic activity of supported gold NPs has explored the redox behaviour of Au NPs [12–13], acid–base properties of gas-phase gold, and gold-oxide [14–16]. To date several theories have been put forward to explore an extraordinary catalytic activity of supported gold NPs; nonetheless these theories are somewhat contentious [22–25]. The outcomes of these theories showed that the size of gold NPs, choice of support, and method of preparation played an important role in delivering a highly efficient catalyst [26].

Pal et al. for the first time introduced catalytic reduction of 4-nitrophenol (4-NP) to 4-aminophenol (4-AP) [27–30]. This reaction takes place in aqueous system on the surface of a catalyst. Reduction of this organic pollutant can be conveniently monitored by decrease of strong UV-visible absorption spectra of 4-nitrophenolate anion at 400 nm [31, 32]. Au nanoparticles supported on Al_2O_3 and SiO_2 are reported to be thermally much more stable than Au nanoparticles on TiO_2. For example, thermal treatment of Au nanoparticles up to 700 °C, on SiO_2, let particles grow from 4 to 6 nm while on TiO_2 from 3 to 13 nm. Also, Al_2O_3 provides a nonreducible support and a nonoxidizing atmosphere for stable supported Au nanoparticle [33]. To the best of our knowledge we obtained lowest effective nobel metal loading as compared to previous reports [33–36].

In the present work, a set of Au/γ-Al_2O_3 catalysts were prepared by successive impregnation method. For this purpose, γ-Al_2O_3 support in granular shape (mesh size = 0.6-1 mm and BET surface area = 175 m^2g^{-1}) was prepared by sol gel route. All the prepared samples were characterized by XRD, surface area analysis, SEM, and FTIR. The aim of this work was to synthesize cost efficient supported gold catalysts with low noble content and evaluate their catalytic activity for the reduction of 4NP to 4AP using SBH as a reducing agent by UV-visible spectroscopy. Interestingly, the prepared catalysts showed excellent activity towards the conversion 4-NP to 4AP, owing to good metal dispersion and metal-support interactions.

2. Experimental

2.1. Materials

Aluminium chloride hexahydrate ($AlCl_3.6H_2O$, Merck, 99.9%), ammonium hydroxide (NH_4OH, Fisher, 33%), and gold chloride trihydrate ($HAuCl_4.3H_2O$, Merck, 99.9%) were used as precursors. Distilled water with the ionic conductivity $\leq$10 µS cm^{-1} was used in the preparation of all aqueous solutions.

2.2. Preparation of supported catalysts

Alumina support was produced by sol gel method using 0.4M $AlCl_3.6H_2O$ solution and 0.4M NH_4OH solution. The initial pH of NH_4OH solution was recorded as 12. $AlCl_3.6H_2O$ solution and was added to NH_4OH solution slowly with continuous stirring until alumina sol was obtained at pH 8. Alumina sol was aged in heating oven at 80 °C for 48 h. Under vacuum filtration gel was washed with deionized water to remove the impurities (i.e. Cl^-, Na^+, NH_4^+ etc.). If these impurities remain in the support, they can affect the efficiency of catalyst. Alumina gel was converted to the granules by a method described earlier [37–38]. In order to obtain gamma phase, granules were heat treated in programmable muffle furnace up to 750 °C for 16 h. Granular support (γ-$Al_2O_{3)}$ was obtained having mesh size, between 0.6 and 1 mm and BET surface area of 175 m^2g^{-1}.

A series of Au/γ-Al_2O_3 catalysts were prepared by wet impregnation method with composition of 0.2%, 0.4%, 0.6%, 0.8%, 1% by weight. Impregnation was accomplished on predried γ-Al_2O_3 granular support using

required volume of $HAuCl_4$ precursor. All catalysts were soaked overnight, dried in oven at 120 °C for 2 h and further calcined at 550 °C for 3 h. Finally, catalysts were reduced in H_2 gas (99.99 %) flow at 550 °C for 3 h.

2.3. Characterization

X-ray diffraction (XRD) patterns of the synthesized materials packed in an aluminium glass holder were recorded at room temperature using Philips PW-1840 diffractometer with CuKα radiation (λ = 0.154 nm) in 2θ range of 20°–80°with scan rate of 0.01 θ s^{-1}.

Surface area analysis (SAA) of supported catalyst was carried out on KELVIN 1042. Degassing of the samples was carried out at 250 °C with N_2 as carrier gas. BET surface area was obtained from nitrogen adsorption–desorption isotherms measured at liquid nitrogen temperature (−196 °C). Pore size and total pore volume were obtained by employing BJH method.

Fourier transform infrared (FTIR) spectroscopy analysis was carried out on Thermo Scientific, model 6700FTIR made of USA and the technique applied was ATR (attenuated total reflectance) at a range of 400–4000cm^{-1}. Scanning electron microscopy (SEM) was used to examine surface morphology of the samples on JEOL-JED 2300 instrument and on TEM Philips TEM CM12. A UV-visible spectrophotometer (UV-1601 Shimadzu spectrophotometer) with wavelength range of 190–1100 nm was utilized to collect spectral data.

2.4. Catalytic activity test

The catalytic performance of Au/γ-Al_2O_3 catalysts was evaluated with the help of a well-studied reaction of conversion of 4NP to 4AP using SBH as a reducing agent and UV-visible spectra were recorded during the reaction [32]. In a typical reaction, 5 mg of sample in a standard quartz cuvette was taken and then 100 µL of 1mM 4NP solution was added. The volume was adjusted to 3.5 mL with water and finally ice-cold SBH (100 µL, 100 mM) was added to the above quartz cuvette. The decrease in absorbance of 4NP was recorded with a time interval of 3–5 min (according to the reaction conditions). Rate constants were observed to be dependent upon the wt% of Au nanocatalyst and temperature. The catalytic reaction was carried out at various temperatures to calculate kinetic parameters (rate constant and activation energy).

3. Results and discussion

3.1. Characterization of support and catalysts

The nitrogen adsorption-desorption isotherms (Figure 1a) of 0.6Au/γ-Al_2O_3 sample with type IV shape designated the presence of mesopores with uniform pore size distribution [37, 38]. Table 1 presents the composition, BET surface area, pore volume, average pore diameter, and crystallite sizes of γ-Al_2O_3 support and Au/γ-Al_2O_3 catalysts. Figure 1b shows unimodal distribution of pore for Au/γ-Al_2O_3 catalyst which exhibited with maxima centred at ~7 nm. BET surface area and pore volume of Au catalysts were found to decrease with respect to γ-Al_2O_3 support. It can be correlated to occlusion of alumina pores with Au particles during impregnation process. In addition, with further increase in metal content, BET surface area of the catalysts was examined to decrease which might be due to metal-on-metal deposition besides the blockage of alumina pores with metal. After the deposition of gold NPs on γ-Al_2O_3 support the surface area of the support decreased from 175 m^2g^{-1} to 129 m^2g^{-1} and pore volume decreased from 0.47 cm^3g^{-1} to 0.310 cm^3g^{-1}. This reduction in surface area and pore volume of the pure support after metal loadings provides an evidence of the successful deposition of the gold NPs by impregnation method.

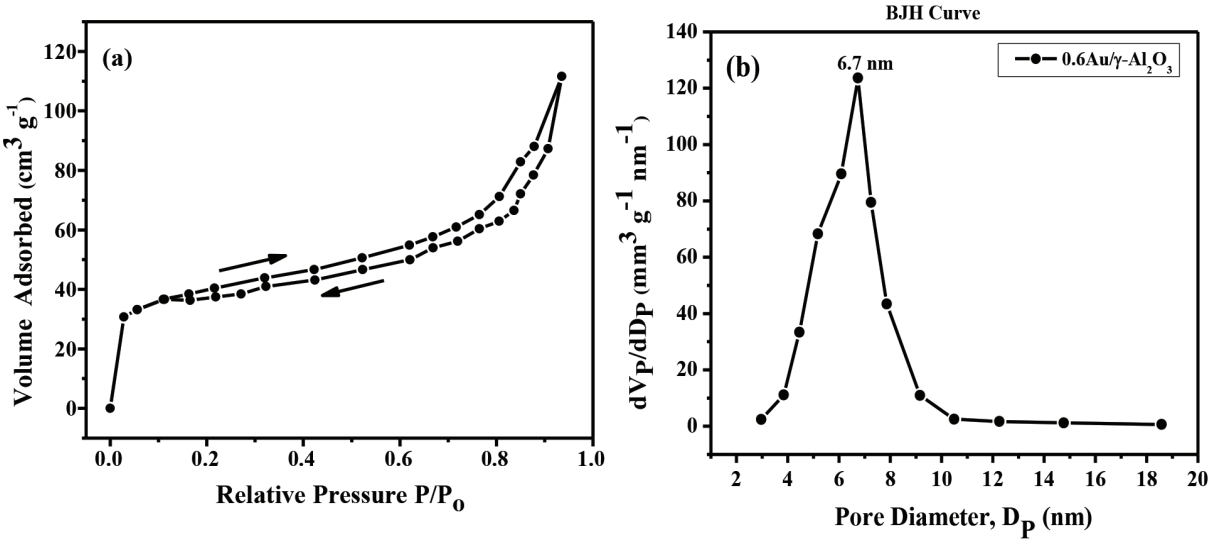

Figure 1. Adsorption-desorption isotherms (a) and pore size distribution of 0.6Au/γ-Al_2O_3 catalyst using BJH method (b).

Table 1. Table 1 presents the composition, BET surface area, pore volume, average pore diameter, and crystallite sizes of γ-Al_2O_3 support and Au/γ-Al_2O_3 catalysts.

Samples	Composition	Surface properties		
	Au[a](wt%)	S_A^b (m^2g^{-1})	V_P^C (cm^3g^{-1})	D_p^d (nm)
$\gamma-Al_2O_3$	0	175.0	0.47	7.8
0.2Au/γ-Al_2O_3	0.2	165.3	0.45	6.9
0.4Au/γ-Al_2O_3	0.4	155.1	0.43	6.8
0.6Au/γ-Al_2O_3	0.6	140.5	0.38	6.7
0.8Au/γ-Al_2O_3	0.8	135.8	0.35	6.3
1Au/γ-Al_2O_3	1	129.2	0.31	6.0

[a]Nominal Au metal content, [b]BET specific surface area, [c]Pore volume, [d]Pore diameter determined by surface area analyser.

Figure 2 shows XRD patterns of Al_2O_3 support and Au/γ-Al_2O_3 catalysts. The significant peaks in XRD pattern of γ-Al_2O_3 were appeared at 2θ ~37°, 46°, and 66° having (311), (400), and (440) hkl values, respectively. These values matched with standard ICDD Card No 00-001-1303 thus indicating the formation of cubic and pure gamma phase Al_2O_3 NPs. For all Au catalysts, no additional XRD peaks were observed besides the significant peaks of γ-Al_2O_3 thus showing either complete incorporation of Au NPs into γ-Al_2O_3 pores or metal particles are too small which could not be detected by XRD. The crystallite sizes (D_{XRD}) of Au/γ-Al_2O_3 catalysts were attained by Debye Scherrer formula:

$$D_{XRD}\ (\text{nm}) = K\lambda/\beta\cos\theta,$$

where K is particle shape factor (0.9 for cubic system), λ is wavelength of X-ray beam (0.154 nm), β is peak broadening (FWHM), and θ is diffraction angle.

D_{XRD} values of all samples were calculated by using high intensity diffraction peak and were found ~6 nm.

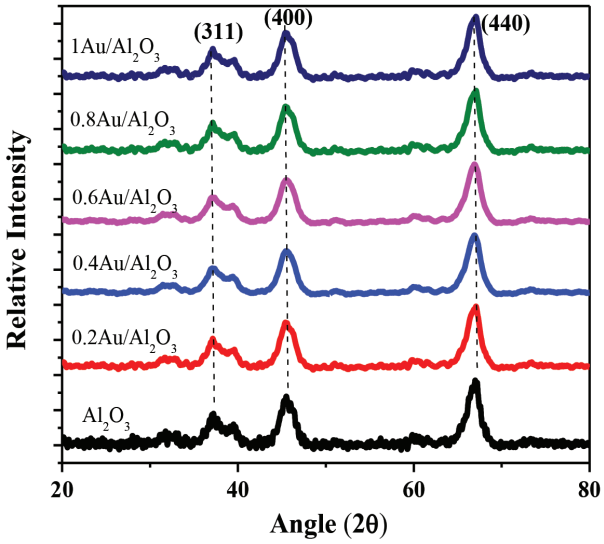

Figure 2. XRD patterns of γ-Al2O3 support and Au/γ-Al2O3 catalysts.

To investigate the morphology of synthesized materials, SEM images were taken. Figure 3a presents SEM image of γ-Al_2O_3 support calcined at 750 °C. With a coarse surface, γ-Al_2O_3 was observed having particles of irregular size and shape. In contrast, 0.6Au/γ-Al_2O_3 catalyst (Figure 3b-3d) presented homogenous distribution of Au NPs over the surface of γ-Al_2O_3 support at different resolutions. Au particles were found spherical in shape having uniform size. Here, high metal dispersion of this optimal composition was corresponded for its excellent activity towards conversion of 4NP to 4AP. Figure 3e shows TEM image of 0.6Au/γ-Al_2O_3 showing AuNPs of ~6 ±2 nm.

FTIR spectra of pure γ-Al_2O_3 along with Au supported analogues are presented in Figure 4. In pure γ-Al_2O_3 the absorption band around 3400 cm^{-1} can be ascribed to stretching mode of hydroxyl (OH) group. The peak at 1640 cm^{-1} may be attributed to the bending vibration of weakly bound molecular water. The absorption bands in the region of 600–660cm^{-1} may be attributed to the stretching mode of AlO_4 and AlO_6 while absorption bands below 600 cm^{-1} appeared due to the bending modes of vibrations of AlO_6 groups. In the case of Au/γ-Al_2O_3 catalysts vibrational and stretching modes were affected by Au content in alumina. Au being paramagnetic in character may interfere with electron density on Al = O bond resulting in dilution of electron density on doubly bonded oxygen and reduction in the rigid character of Al = O bond in Al_2O_3. As a consequence, the peak was shifted towards higher wave number i.e. from 600 to 700 cm^{-1}. FTIR, being a very sensitive technique, can detect even small amount of impurity present in the samples. This fact is evident when we compare the FTIR and XRD results in present case, where we did not get new diffraction peaks after depositing gold on alumina support. On the other hand, changes in the FTIR spectra pattern of pure alumina after gold loading were detected. The change in the colour of the Au/γ-Al_2O_3 catalyst with increase in concentration of the deposited gold is evident in the Figure 4. From 0.2wt% loading of Au to 1wt% loading of Au metal content, Au/ γ-Al_2O_3 supported catalyst show a variation from light pink to a reddish pink coloration. This physical change in the colour of Au/γ-Al_2O_3 catalysts is because of the well-known coupling of the Plasmon responses of the attached nanoparticles. As the coverage increases, the average interparticle separation decreases and the above-mentioned coupling increases.

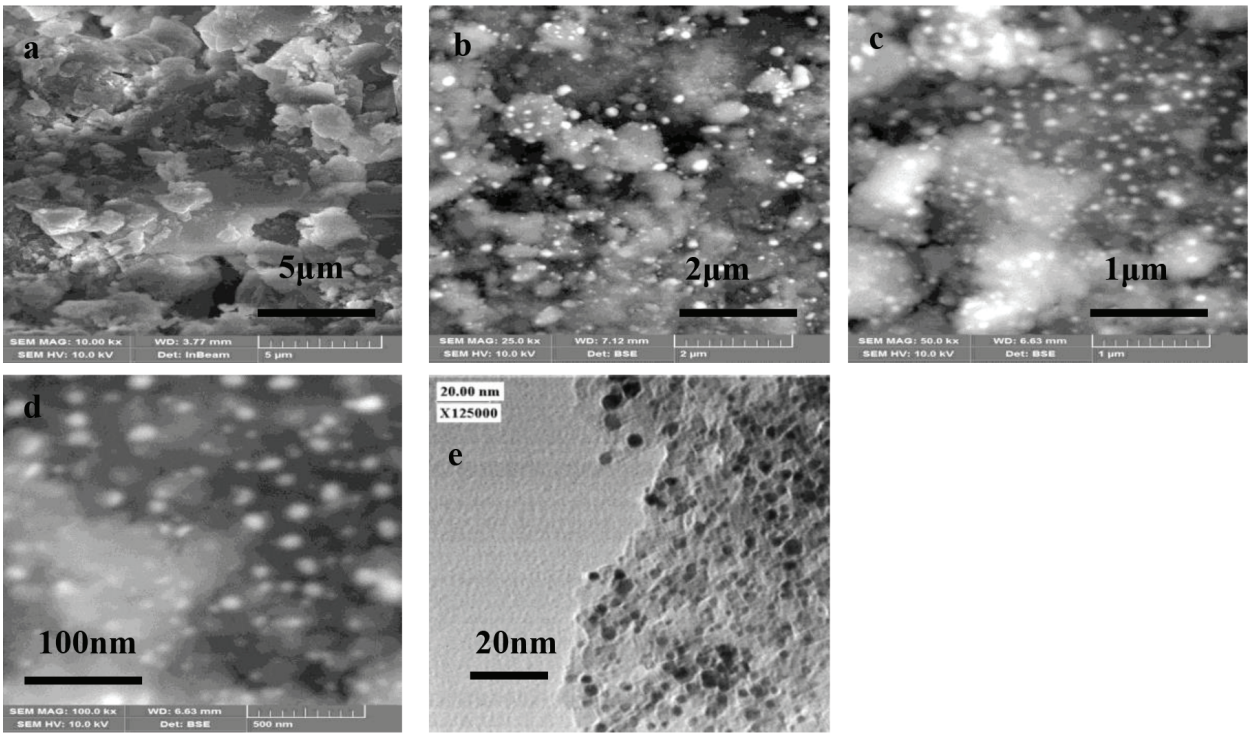

Figure 3. SEM images of synthesized γ-Al_2O_3 support (a), 0.6Au/ γ-Al_2O_3 catalyst (b-d), TEM image of 0.6 wt% Au/γ-Al2O3 catalyst (e).

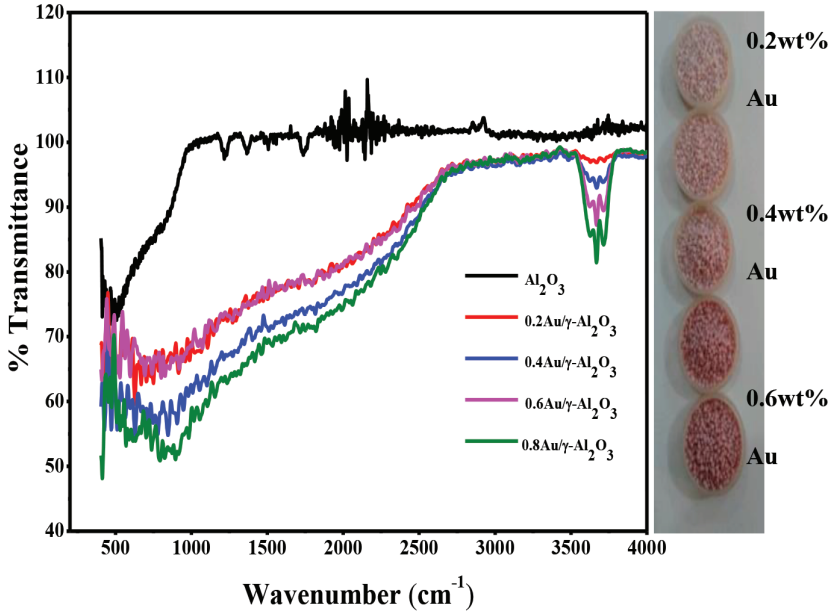

Figure 4. FTIR spectra of γ-Al2O3 and supported Au catalysts.

3.2. Catalytic testing of prepared catalysts

Figure 5 shows the typical UV-visible spectra for the conversion of 4NP to 4AP. A significant decrease in peak intensity was observed upon the conversion. In the spectrum 4- nitrophenol was depicted λ_{max} at ~400 nm and was shifted to ~295 nm during the catalytic reaction thus confirming the formation of 4-aminophenol. The solution (4-Nitrphenol) is light yellow in colour, while 4-aminophenol is colourless. The physical change from light yellow colour to a colourless solution was also examined during the reaction, depicting a complete transformation from 4-nitrophenol to 4-aminophenol. We selected 0.6wt% Au/γ-Al_2O_3 for complete catalytic testing. The reason for selecting this wt% is its ability to catalyse reaction at reduced time as compared to lower (0.2 and 0.4wt%) and higher (0.8 and 1wt%) values. Lower wt% has less deposition of gold nanoparticles and higher wt% block the mesopores in γ-Al_2O_3, which in turn decreases the availability of active sites of nanogold. Thus, out of the 5 prepared catalysts, 0.6Au/ γ-Al_2O_3 was chosen to proceed for further studies.

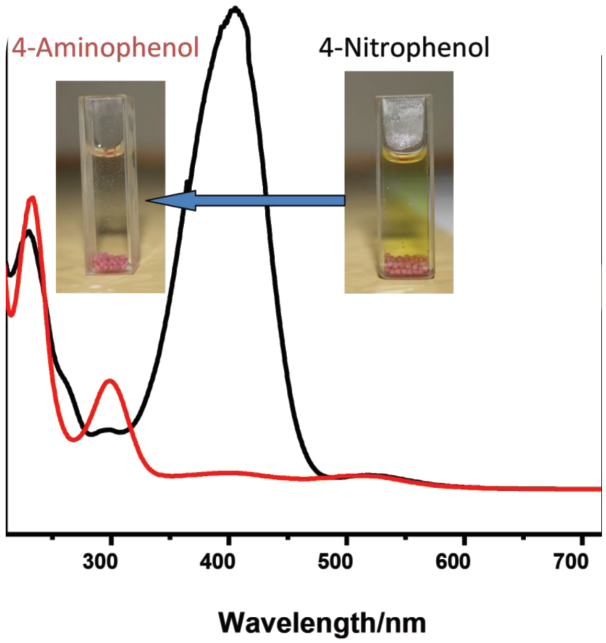

Figure 5. UV-visible spectra for the transformation of 4-nitrophenol to 4-aminophenol over 0.6Au/ γ-Al_2O_3 catalyst.

Figure 6a presents that γ-Al_2O_3 support has no ability to catalyse the reaction at room temperature during different time intervals and even in the entire temperature range studied (higher temperature data is not shown). In the case of 0.6Au/γ-Al_2O_3 catalyst, a significant change in UV-visible absorbance was observed (Figure 6b) for conversion reaction thus depicting the presence of active sites on the surface of 0.6Au/γ-Al_2O_3 catalyst.

Temperature was found to have a pertinent effect on the catalytic performance. The catalysed reaction showed change in its kinetics on increasing the temperature from 25 °C to 40 °C as can be seen in Figure 7a

The rate constant was calculated using the following equation:

$\ln A/A^\circ = -kt$ Eq (1)

$\ln A - \ln A^\circ = -kt$ Eq (2)

$\ln A = \ln A^\circ - kt$ Eq (3)

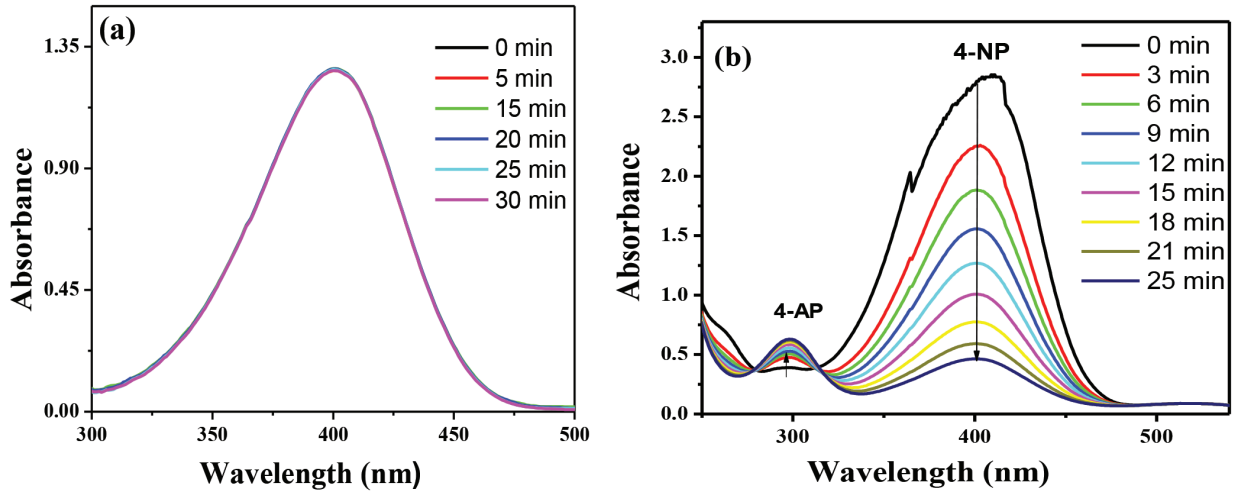

Figure 6. UV-visible spectra for the catalytic activity of γ-Al_2O_3 at different time intervals (a) and 0.6Au/ γ-Al_2O_3 catalyst at 25 °C(b).

Where, A is absorbance of 4-NP at time t, A°is initial absorbance of 4-NP, k is the rate constant, and t is the time interval for UV-visible data collection.

The plot of ln A versus t (Figure 7a) at different temperatures produces a straight line with the slope equivalent to rate constant.

Table 2 presents the rate constant values of the reaction catalysed by Au/γ-Al_2O_3 catalyst at different temperatures.

The rate constant value was observed to increase 5.4 times on increasing the temperature from 25 °C to 40 °C. The activation energy (E_a) was calculated using Arrhenius equation.

$$\mathbf{k = A \exp(-E_a/RT)\ Eq\ (4)}$$

Figure 7b shows the Arrhenius plot of rate constant versus the reciprocal of temperature (both in logarithmic scale) with a straight line. The activation energy was found to be 97 $Kjmol^{-1}$. This value of E_a is high as compared to the E_a for free colloidal suspension of gold nanoparticles as given in our previous results .[31,39]. Although gold NPs deposited on γ-Al_2O_3 were well dispersed as can be seen in Figures 3b-3e, still all the active sites of these supported gold NPs were not available for catalysis. Since we see how the physical state (colloidal or supported) of a catalyst affects its catalytic performance, we can conclude that size and physical state of the catalyst play a very crucial role in their catalytic performance.

Table 2. Kinetic parameters of Au/γ-Al_2O_3 catalyst.

Sample	Temperature (°C)	k $\times 10^{-4}$ (min^{-1})	Ea ($kJmol^{-1}$)
0.6Au/γ-Al_2O_3	25	1.2 $\pm$1 $\times$ 10^{-5}	97 $\pm$14
	30	2.0 $\pm$3 $\times 10^{-5}$	
	35	3.9 $\pm$2 $\times 10^{-5}$	
	40	7.4 $\pm$5 $\times$ 10^{-5}	

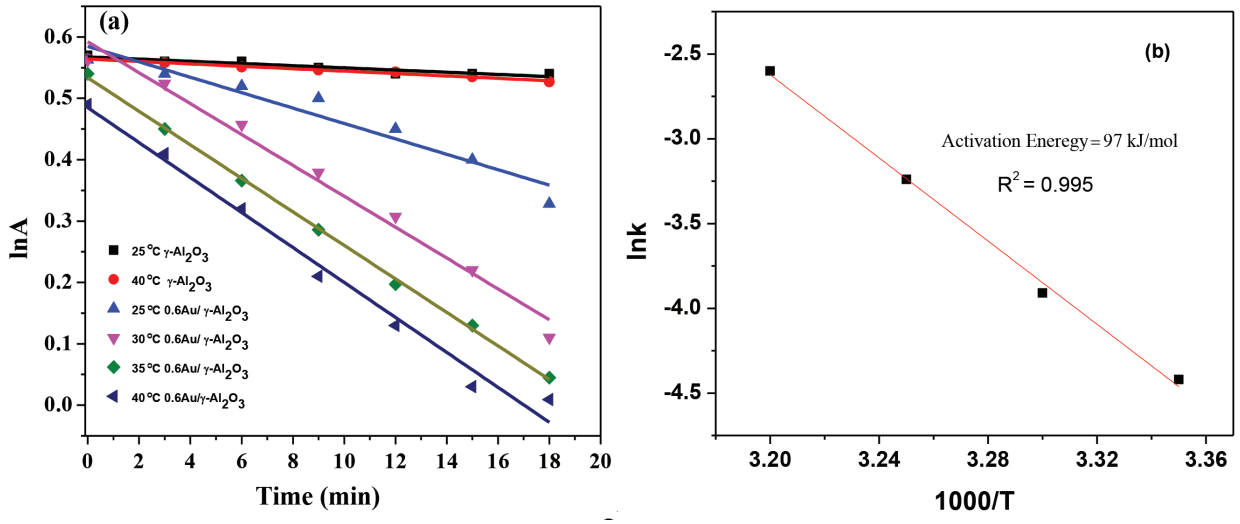

Figure 7. lnA vs t plot for the conversion reaction over γ-Al_2O_3 support and prepared Au/γ-Al_2O_3 catalysts (a) and Arrhenius plot for the activity of 0.6Au/γ-Al_2O_3 catalyst at different temperatures(b).

Supported gold catalyst was well stable during the course of reaction and even after many cycles in comparison to the reported colloidal alloy nanoparticles [39], which show aggregation during and after the catalysed reaction. It is reported that capping material is usually stripped off during the catalytic reaction, so this may contribute towards the nanocatalyst aggregation which is not observed in the present case for the supported catalyst. Present catalyst is also recyclable, it was used 6 times with appreciable efficiency (Figure 8). The AuNPs supported on the surface of mesoporous γ-Al_2O_3 were found to be stable and did not leach out into the solution after heating at 60 °C for 1h. This was confirmed by taking UV-visible of solution which shows no SPR for free AuNPs or gold salt, also SEM imaging, which showed no free AuNPs in the solution (Figure 3e).

The dependence of the reduction of 4-NP by BH as a function of temperature can be modelled in terms of Langmuir-Hinshelwood model [40–42]. According to this model both reactants must be adsorbed to the surface of the nanocatalyst to react and this reaction was found to be kinetics controlled where the transportation of the reactants through the solution was not the rate determining step, rather the formation of 4-AP was the rate determining step. The adsorbed species can then react, and the product will desorb from the surface of supported gold catalyst (Figure 9). Comparative performance of Au/γ-Al_2O_3 catalyst with available literature is compiled in Table 3.

4. Conclusions

In the present work, a sol–gel method was utilized to synthesize mesoporous γ-Al_2O_3 in granular shape with BET surface area of 175 m^2g^{-1}, which was reduced to 125 m^2g^{-1} after gold deposition. Au/γ-Al_2O_3 catalysts with 0.2–1wt% metal contents were prepared via impregnation method. The results of SAA indicated a decrease in BET specific surface area of Au catalysts due to occlusion of γ-Al_2O_3 pores with metal particles while pore diameter increased up to 8 nm at the expense of sintering process. XRD results depict the formation of single phase γ-Al_2O_3 NPs. SEM depicted a uniform dispersion of Au particles on the surface of γ-Al_2O_3 support. The metal particles were found spherical. The catalytic activity of Au/γ-Al_2O_3 (0.6wt%) catalyst

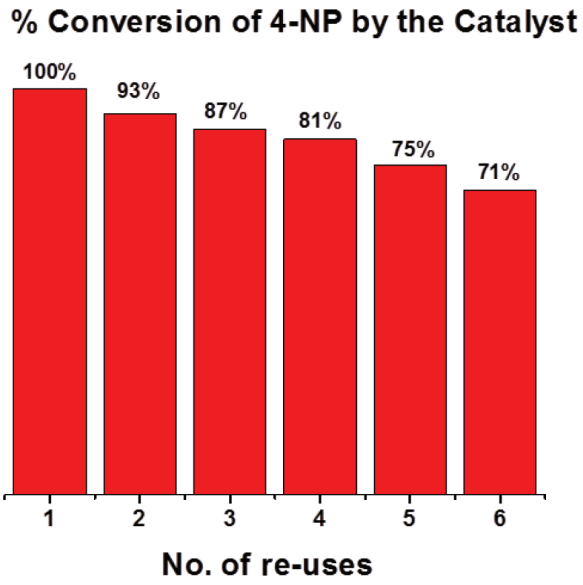

Figure 8. Recyclability of 0.6Au/γ-Al2O3 catalyst over many uses.

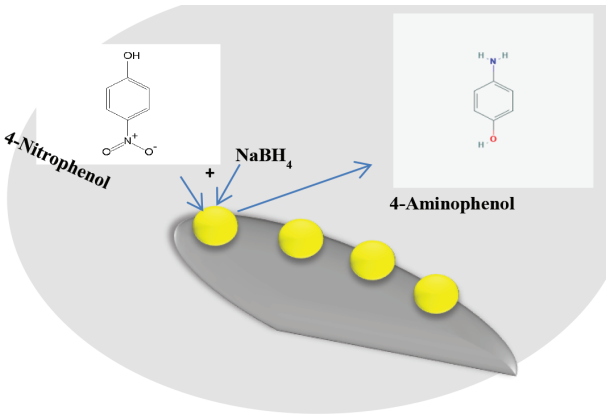

Figure 9. Mechanism of 4-NP reduction on the surface of 0.6Au/γ-Al_2O_3 catalyst following Langmuir Hinshelwood model where both 4-NP and $NaBH_4$ adsorb at the surface of nanocatalyst and 4-AP as a product desorb.

Table 3. Comparison of wt% Au loading and catalytic activity of our work with literature.

Sample code	Reaction studied	Wt% Au loading	Rate constant (min^{-1})	Year	Reference
Au/Al_2O_3	$[Fe(CN)_6]^{3-}$ with $(S_2O_3)^{2--}$	3.6	0.0017	2012	19
Au/Starch	4-Nitrophenol reduction with $NaBH_4$	4.32	0.0081	2017	36
Au/Carbon	4-Nitrophenol reduction with $NaBH_4$	2	0.660	2019	35
Au/Al_2O_3	Thermal stability	4	-	2019	33
Au/Al_2O_3	4-Nitrophenol reduction with $NaBH_4$	0.6	0.00012	2020	This work

was evaluated for reduction of 4NP to 4AP at 4 temperatures i.e. 25, 30, 35, and 40 °C and UV-visible spectra were recorded. γ-Al_2O_3 support exhibited no activity for the conversion reaction while Au catalyst showed a significant change in UV-visible absorbance with rate constant 1.2×10^{-4} min^{-1}. Use of low noble metal content made the process cost effective and efficient at the same time.

Acknowledgements

This work was supported by Higher Education Commission (HEC) of Pakistan and Department of Chemistry of Quad-i-Azam University, Islamabad, Pakistan.

References

1. Haruta M, Kobayashi T, Sano H, Yamada N. Novel gold catalysts for the oxidation of carbon monoxide at a temperature far below 0 °C. Chemistry Letters 1987; 16 (2): 405-408.
2. Haruta M, Tsubota S, Kobayashi T, Kageyama H, Genet MJ et al. Low-temperature oxidation of CO over gold supported on TiO2, α-Fe2O3, and Co3O4. Journal of Catalysis 1993, 144(1):175-192.
3. Tan X, Deng W, Liu M, Zhang Q, Wang Y. Carbon nanotube-supported gold nanoparticles as efficient catalysts for selective oxidation of cellobiose into gluconic acid in aqueous medium. Chemical Communications 2009; (46): 7179-7181.
4. Tuzovskaya I, Lima E, Bosch P, Bogdanchikova N, Pestryakov A et al. Influence of cation nature on stabilization of gold nanospecies in mordenites. Journal of nanoscience and nanotechnology 2011; 11 (6): 5469-5475.
5. Yuan Y, Kozlova AP, Asakura K, Wan H, Tsai K et al. Supported Au catalysts prepared from Au phosphine complexes and as-precipitated metal hydroxides: characterization and low-temperature CO oxidation. Journal of Catalysis 1997; 170 (1): 191-199.
6. Zhang J, Liu X, Hedhili MN, Zhu Y, Han Y. Highly selective and complete conversion of cellobiose to gluconic acid over Au/Cs2HPW12O40 nanocomposite catalyst. ChemCatChem 2011; 3 (8): 1294-1298.
7. Erlt G, Knözinger H, Weitkamp J. Handbook of Heterogenous Catalysis. Weinheim, Germany: Wiley-VCH, 1997.
8. Haruta M, Yamada N, Kobayashi T, Iijima S. Gold catalysts prepared by coprecipitation for low-temperature oxidation of hydrogen and of carbon monoxide. Journal of Catalysis 1989; 115 (2): 301-309.
9. Bond G, Thompson D. Gold catalysis. Catalysis Reviews-Science and Engineering 1999; 41: 319-388.
10. Haruta M. Gold as a novel catalyst in the 21st century: Preparation, working mechanism and applications. Gold Bulletin 2004; 37 (1-2): 27-36.
11. Lima E, Guzmán-Vargas A, Méndez-Vivar J, Pfeiffer H, Fraissard J. Fe-ZSM-5 catalysts: preparation in organic media, Fe-particle morphology and NO x reduction activity. Catalysis Letters 2008; 120 (3-4): 244-251.
12. Zhdanov VP, Kasemo B. Diffusion-limited reaction kinetics in nanofabricated porous model catalysts. Catalysis Letters 1998; 50 (3-4): 131-134.
13. Shaikhutdinov SK, Meyer R, Naschitzki M, Bäumer M, Freund HJ. Size and support effects for CO adsorption on gold model catalysts. Catalysis Letters 86: 211-219.
14. Weil D, Wilkins CL. A comparison of the ion-molecule reactions of Group 11 metal ions with alcohols. Journal of the American Chemical Society 1985; 107 (25): 7316-7320.
15. Kung HH, Kung M, Costello C. Supported Au catalysts for low temperature CO oxidation. Journal of Catalysis 2003; 216 (1-2): 425-432.
16. Al-Daous MA, Manda AA, Hattori H. Acid–base properties of γ-Al2O3 and MgO–Al2O3 supported gold nanoparticles. Journal of Molecular Catalysis A: Chemical 2012; 363: 512-520.
17. Huang J, Lima E, Akita T, Guzmán A, Qi C et al. Propene epoxidation with O2 and H2: Identification of the most active gold clusters. Journal of Catalysis 2011; 278 (1): 8-15.
18. Lee I, Joo JB, Yin Y, Zaera F. A yolk@ shell nanoarchitecture for Au/TiO2 catalysts. Angewandte Chemie International Edition 2011; 50 (43): 10208-10211.
19. Rashidi F, Lima E, Rashidi H, Rashidi A, Guzmán A. Cooperative effect of gold nanoparticles with CUS aluminium from nanoalumina support in the catalysis of an electron transfer reaction. Applied Catalysis A: General 2012; 417: 129-136.
20. Villa A, Chan-Thaw CE, Veith GM, More KL, Ferri D et al. Au on nanosized NiO: a cooperative effect between Au and nanosized NiO in the base-free alcohol oxidation. ChemCatChem 2011; 3 (10): 1612-1618.

21. Zhu H, Liang C, Yan W, Overbury SH, Dai S. Preparation of highly active silica-supported Au catalysts for CO oxidation by a solution-based technique. The Journal of Physical Chemistry B 2006; 110 (22): 10842-10848.
22. Carrettin S, Concepción P, Corma A, Lopez Nieto JM, Puntes VF. Nanocrystalline CeO2 increases the activity of Au for CO oxidation by two orders of magnitude. Angewandte Chemie International Edition 2004; 43 (19): 2538-2540.
23. Centomo P, Zecca M, Di Noto V, Lavina S, Bombi GG et al. Characterization of synthetic iron oxides and their performance as support for Au catalysts. ChemCatChem 2010; 2 (9): 1143-1149.
24. Ivanova S, Pitchon V, Petit C, Caps V. Support effects in the gold-catalyzed preferential oxidation of CO. ChemCatChem 2010; 2 (5): 556-563.
25. Schubert MM, Plzak V, Garche J, Behm RJ. Activity, selectivity, and long-term stability of different metal oxide supported gold catalysts for the preferential CO oxidation in H2-rich gas. Catalysis Letters 2001; 76 (3-4): 143-150.
26. Somodi F, Borbath I, Hegedűs M, Lazar K, Sajo IE et al. Promoting effect of tin oxides on alumina-supported gold catalysts used in CO oxidation. Applied Surface Science 2009; 256 (3): 726-736.
27. Corbett JF. An historical review of the use of dye precursors in the formulation of commercial oxidation hair dyes. Dyes and Pigments 1999; 41 (1-2): 127-136.
28. Pradhan N, Pal A, Pal T. Silver nanoparticle catalyzed reduction of aromatic nitro compounds. Colloids and Surfaces A: Physicochemical and Engineering Aspects 2002; 196 (2-3): 247-257.
29. Rode C, Vaidya M, Chaudhari R. Synthesis of p-aminophenol by catalytic hydrogenation of nitrobenzene. Organic Process Research & Development 1999; 3 (6): 465-470.
30. Saha S, Pal A, Kundu S, Basu S, Pal T. Photochemical green synthesis of calcium-alginate-stabilized Ag and Au nanoparticles and their catalytic application to 4-nitrophenol reduction. Langmuir 2009; 26 (4): 2885-2893.
31. Mahmoud M, Saira F, El-Sayed M. Experimental evidence for the nanocage effect in catalysis with hollow nanoparticles. Nano Letters 2010; 10 (9): 3764-3769.
32. Praharaj S, Nath S, Ghosh SK, Kundu S, Pal T. Immobilization and recovery of Au nanoparticles from anion exchange resin: resin-bound nanoparticle matrix as a catalyst for the reduction of 4-nitrophenol. Langmuir 2004; 20 (23): 9889-9892.
33. Masoud N, Partsch T, de Jong KP, de Jongh PE. Thermal stability of oxide-supported gold nanoparticles. Gold Bulletin 2019; 52 (2): 105-114.
34. Seker E, Gulari E. Single step sol–gel made gold on alumina catalyst for selective reduction of NOx under oxidizing conditions: effect of gold precursor and reaction conditions. Applied Catalysis A: General 2002; 232 (1-2): 203-217.
35. Molina HR, Muñoz JLS, Leal MID, Reina TR, Ivanova S et al. Carbon supported gold nanoparticles for the catalytic reduction of 4-nitrophenol. Frontiers in Chemistry 2019, 7.
36. Chairam S, Konkamdee W, Parakhun R. Starch-supported gold nanoparticles and their use in 4-nitrophenol reduction. Journal of Saudi Chemical Society 2017; 21 (6): 656-663.
37. He L, Huang Y, Wang A, Liu Y, Liu X et al. Surface modification of Ni/Al2O3 with Pt: highly efficient catalysts for H2 generation via selective decomposition of hydrous hydrazine. Journal of Catalysis 2013; 298: 1-9.
38. Karim M, Rahman M, Miah M, Ahmad H, Yanagisawa M et al. Synthesis of γ-Alumina Particles and Surface Characterization. Open Colloid Science Journal 2011; 4: 32-36.
39. Mehmood S, Janjua NK, Saira F, Fenniri H. AuCu@ Pt nanoalloys for catalytic application in reduction of 4-nitrophenol. Journal of Spectroscopy 2016; 1-8.
40. Herves P, Pérez-Lorenzo M, Liz-Marzán LM, Dzubiella J, Lu Y et al. Catalysis by metallic nanoparticles in aqueous solution: model reactions. Chemical Society Reviews 2012; 41 (17): 5577-5587.

41. Wunder S, Lu Y, Albrecht M, Ballauff M. Catalytic activity of faceted gold nanoparticles studied by a model reaction: evidence for substrate-induced surface restructuring. Acs Catalysis 2011; 1 (8): 908-916.

42. Wunder S, Polzer F, Lu Y, Mei Y, Ballauff M. Kinetic analysis of catalytic reduction of 4-nitrophenol by metallic nanoparticles immobilized in spherical polyelectrolyte brushes. The Journal of Physical Chemistry C 2010; 114 (19): 8814-8820.